Low-lying structure and weak-coupling multiplets of odd-mass Te isotopes below and beyond the neutron magic number $N = 82$

Hui Jiang [1,*] Chang-hao Mao,[1,2] Yang Lei [3] Guan-Jian Fu [4] and Zhen-Zhen Qin[5]

[1]*School of Science, Shanghai Maritime University, Shanghai 201306, China*

[2]*Merchant Marine College, Shanghai Maritime University, Shanghai 201306, China*

[3]*School of Nuclear Science and Technology, Southwest University of Science and Technology, Mianyang 621010, China*

[4]*School of Physics Science and Engineering, Tongji University, Shanghai 200092, China*

[5]*School of Mathematics and Physics, Southwest University of Science and Technology, Mianyang 621010, China*

(Received 15 January 2024; revised 16 May 2024; accepted 18 June 2024; published 10 July 2024)

The low-lying level schemes, $E2$ transitional rates, electrical quadrupole moments Q, and magnetic dipole moments μ of odd-mass Te isotopes with mass number from 129–139 are calculated within the framework of the nucleon-pair approximation of the shell model by using the standard multipole-multipole interaction in a large truncated space. Good agreement is obtained between the calculated results and experimental data. The dominant configurations in collective nucleon-pair basis of low-lying yrast states in $^{129-133}$Te and $^{135-139}$Te are analyzed in detail. The possible weak-coupling multiplets in these nuclei are probed by investigating the corresponding relative excitation energy, wave function, $E2$ transition rates, electric quadrupole moments Q, and magnetic dipole moment μ. $E2$ ground-state transitions of odd-mass nuclei and even-even core are compared, and a similar asymmetry pattern with respect to $N = 82$ is obtained. The electromagnetic moments Q and μ of the $3/2_1^+$, $11/2_1^-$ states in $^{129-133}$Te, and the $7/2_1^-$ state in $^{135-139}$Te are discussed in terms of the overall trend and the contribution of the proton and neutron components.

DOI: 10.1103/PhysRevC.110.014315

I. INTRODUCTION

The study of neutron-rich nuclei in the ^{132}Sn region is one of the hot and challenging topics in nuclear structure and nuclear astrophysics [1–4]. Heavy tellurium (Te) isotopes with mass number A around 130 have two valence protons and several valence neutrons (or neutron holes) outside the ^{132}Sn core. Such nuclei are well worth studying, since they offer relatively simple laboratories for exploring nucleon-nucleon interactions, testing model Hamiltonians, and studying single-particle excitations and collective motions [5,6]. The 2_1^+ levels and $E2$ transitional rates $B(E2, 2_1^+ \to 0_1^+)$ of even-even Te isotopes exhibit asymmetric structural evolutions across the $N = 82$ shell closure, implying different collectivity for valence neutron particles and holes [7,8]. Particle-particle nuclei with $Z > 50$ and $N > 82$ present faster collective development than particle-hole nuclei with $N < 82$ [9,10]. And a shape transition from spherical in ^{136}Te to prolate in ^{140}Te is predicted to take place at ^{139}Te [11]. It is thus interesting to study the low-lying structural evolution of odd-mass heavy Te isotopes with neutron number across the $N = 82$ shell closure.

The energy level of neutron-rich isotopes is one of the observations reflecting nuclear structure information, and has important influence on the modeling of r-process path [12]. Compared with the even-even nuclei, odd-mass nuclei exhibit more extensive and complex band structures. Experimentally, every neutron-hole nuclei of ^{127,129,131,133}Te has a $I_\pi = 3/2^+$ ground state and a low-lying $11/2^-$ β-decaying isomer [13,14]. The high-spin level schemes of odd-mass $^{125-133}$Te have been extended up to 5–6 MeV excitation energies [14–16]; the effects of the proton-pair breaking along the yrast lines [16], as well as the core-excited states [17,18], are analyzed by the shell-model calculations. For the neutron-particle nuclei ^{135,137,139}Te with $N > 82$, available experimental energy levels are relatively scarce. The level scheme of ^{135}Te has been considerably extended up to 6 MeV, but for ^{137}Te and ^{139}Te, energy levels are only extended to 2–3 MeV [19]. The ground states of ^{135,137,139}Te are suggested to have spin and parity $I_\pi = 7/2^-$, from the systematic trend of yrast excitations in $N = 83, 85, 87$ isotones [19]. As the number of valence neutrons beyond the $N = 82$ closed shell increases, level schemes of ^{135,137}Te and ^{139}Te show an excitation pattern characteristic of spherical [20,21] and transitional [11] nuclei, respectively.

The electromagnetic properties provide us with relevant information on the two-body interactions of valence nucleons and detailed single-particle configurations contributing to the nuclear wave function, thereby helping us understand nuclear shell structure. The measurement of electromagnetic properties in this region is a challenging task. So far, the heaviest tellurium nucleus with known magnetic dipole moments (μ) and electric quadrupole moment (Q) is ^{135}Te [22]. The $\mu(11/2_1^-)$ values in neutron-hole Te isotopes with $N < 82$ are negative and become slightly more negative with increasing

*Contact author: huijiang@shmtu.edu.cn

mass number [23]. The observed trends of $\mu(7/2_1^-)$ and $Q(7/2_1^-)$ in $N = 83$ isotones show a negative growth as the proton number Z increases from 52–66, reflecting the effects of valence protons [24]. The $B(E2, 15/2_1^- \rightarrow 11/2_1^-)$ value of ^{135}Te is typical of a vibrational transition [10]; its $B(E2, 19/2_1^- \rightarrow 15/2_1^-)$ value [3.92(20) W.u.] is larger than the $B(E2, 6_1^+ \rightarrow 4_1^+)$ [2.05(4) W.u.] of ^{134}Te, which can be understood as an effect of the mixing in the $15/2_1^-$ state of the $(\pi g_{7/2}^2)4^+ \otimes \nu f_{7/2}$ and $(\pi g_{7/2}^2)6^+ \otimes \nu f_{7/2}$ couplings [25].

The purpose of this paper is to apply the nucleon-pair approximation (NPA) [26,27] of the shell model to study the low-lying structures and possible weak-coupling multiplets for odd-mass $^{129-139}$Te isotopes. The NPA is one natural and efficient truncation scheme of the shell model. It can treat even-even, odd-mass, and odd-odd nuclei on the same footing. In the past 20 years, the NPA has made a lot of progress in the study of medium and heavy nuclei [28–36]. Traditional J-scheme version of the NPA adopts basis states constructed by stepwise couplings of nucleon pairs with given spin; the dimension of the collective nucleon-pair subspace is small, thus providing a simple and illuminating picture of the nuclear structure under investigation. There have also been a number of important developments in the model itself in recent years, including isospin symmetry [37], particle-hole excitations [38], m-scheme versions [39], deformation [40], and state-of-the-art version of the NPA (which combines the advantages of both J-scheme and m-scheme versions) [41].

In 2007, the NPA calculation of odd-mass Sn, Te, Xe, Ba, Ce, Sb, I, Cs, and La isotopes in this region was performed in the SD-pair truncated space with the strengths of quadrupole pairing and quadrupole-quadrupole interactions varying with the mass number [32]. The excited energies of low-lying yrast states for $^{129-135}$Te agree well with the experiment, but those of $^{137-139}$Te differ from the experiment to some extent. This calculation demonstrated that S and D pairs play an important role in the low-lying states for $^{129-135}$Te. However, due to the faster collective development in the $N > 82$ region, $^{137-139}$Te require a larger truncated space to describe their low-lying states. After 2007, with the improvement of experimental facilities, experimental energy levels and electromagnetic properties in this region have been updated. At the same time, our computing power has also been greatly improved. Therefore, in this paper, the low-lying structures of odd-mass Te nuclei are studied in a large truncated space ($S_\pi D_\pi G_\pi I_\pi + S_\nu D_\nu K_\nu$ pairs for $N < 82$ and $S_\pi D_\pi G_\pi I_\pi + S_\nu D_\nu G_\nu I_\nu K_\nu$ pairs for $N > 82$) according to the single-particle energies. Due to the larger configuration space and better phenomenological interactions, our results agree better with the experimental values, and more low-lying states with high spin can be discussed in this paper. Compared with the previous work in 2007, this paper not only describes and predicts more low-lying energy levels, $E2$ transition rates, electric quadrupole moments Q, and magnetic dipole moments μ, but also focuses on the dominant configuration of wave function, the weak-coupling multiplet, and the evolution of electromagnetic properties. In particular, the data association between excited energy, $B(E2)$ transition, Q, and μ is used to find more evidence for weak-coupling effects in Te isotopes. This is important for understanding the low-lying structures of nuclei in this region.

This paper is organized as follows. In Sec. II we present a brief introduction to the NPA, including the model space, the Hamiltonian, the transition operators, and parametrization of our calculations. In Sec. III we present and discuss our calculated energy spectra, $E2$ transitional rates, electrical quadrupole moments Q, and magnetic dipole moments μ, with our focus on the dominant configuration, the evolution of electromagnetic properties with mass number, and possible weak-coupling multiplets in detail. The summary and conclusion are given in Sec. IV.

II. FORMULATION OF THE NPA

In this section, we present the model space, the Hamiltonian, the transition operators, and parametrization of our calculations. The building blocks of the model space are collective nucleon-pair basis states. For an even system with $2N$ valence protons or neutrons, we assume that all the valence nucleons are coupled to collective nucleon pairs $A_\sigma^{r\dagger}$ with angular momentum $r = 0, 2, 4, 6, 8$ (corresponding to S, D, G, I, and K pairs). $\sigma = \pi, \nu$ is the index of proton and neutron degrees of freedom, respectively. Then the collective nucleon-pair basis state with total angular momentum J_N for an even system is constructed by coupling N collective nucleon pairs $r_1, r_2 \cdots r_N$ stepwise $[\cdots (A^{r_1\dagger} \times A^{r_2\dagger})^{J_2} \times \cdots \times A^{r_N\dagger}]_\sigma^{J_N}|0\rangle$. Similarly, for an odd system with $2N + 1$ valence protons or neutrons, the collective nucleon-pair basis state is given by successively coupling the N nucleon pairs to the unpaired nucleon in a single j_σ orbit as $\{\cdots [(C_{j_\sigma}^\dagger \times A^{r_1\dagger})^{J_1} \times A^{r_2\dagger}]^{J_2} \times \cdots \times A^{r_N\dagger}\}_\sigma^{J_N}|0\rangle$. Here, $C_{j_\sigma}^\dagger$ is the single-particle creation operator in the j_σ orbit. J_N (half-integer) denotes the total angular momentum for the $2N + 1$ nucleons. The combination of proton and neutron collective nucleon-pair basis states forms a complete set of nonorthonormal but linearly independent many-pair basis states.

The Hamiltonian is chosen to have the phenomenological and separable form as follows:

$$\begin{aligned} H = & \sum_{j_\sigma} \epsilon_{j_\sigma} C_{j_\sigma}^\dagger C_{j_\sigma} \\ & - \sum_\sigma \left(G_\sigma^0 \mathcal{P}_\sigma^{(0)\dagger} \cdot \mathcal{P}_\sigma^{(0)} + G_\sigma^2 \mathcal{P}_\sigma^{(2)\dagger} \cdot \mathcal{P}_\sigma^{(2)} \right) \\ & - \sum_\sigma \kappa_\sigma Q_\sigma \cdot Q_\sigma + \kappa_{\pi\nu} Q_\pi \cdot Q_\nu, \end{aligned} \tag{1}$$

where $\mathcal{P}_\sigma^{(0)}$, $\mathcal{P}_\sigma^{(2)}$, and Q_σ are the pairing and quadrupole operators, respectively. ϵ_{j_σ} is the single-particle energy. G_σ^0, G_σ^2, κ_σ, and $\kappa_{\pi\nu}$ are the two-body interaction strengths corresponding to monopole, quadrupole pairing, and quadrupole-quadrupole interactions between valence nucleons. The adopted single-particle energies and two-body interaction strengths are listed in Table I. Among them, the single-particle energies are obtained from the experimental excitation energies [19] of ^{133}Sb (for proton ϵ_{j_π}), ^{131}Sn (for neutron-hole ϵ_{j_ν}), and ^{133}Sn (for neutron-particle ϵ_{j_ν}) except for the neutron $h_{9/2}$ orbital. For this orbital, it is assumed that $\epsilon_{h_{9/2}}$ changes with

TABLE I. Adopted single-particle energies ϵ_{j_σ} and two-body interaction strengths G^0_σ, G^2_σ, κ_σ, and $\kappa_{\pi\nu}$. $\sigma = \pi, \nu$ stands for proton and neutron, respectively. Definition of the $\epsilon_{h_{9/2}}$ is given in the text. ϵ_{j_σ} and G^0_σ are in unit of MeV; G^2_σ, κ_σ and $\kappa_{\pi\nu}$ are in MeV/r_0^4 with $r_0^2 = 1.012A^{\frac{1}{3}}$ fm^2.

	j_π	$s_{1/2}$	$d_{3/2}$	$d_{5/2}$	$g_{7/2}$	$h_{11/2}$	
	ϵ_{j_π}	2.990	2.440	0.962	0.000	2.792	
	j_ν	$s^{-1}_{1/2}$	$d^{-1}_{3/2}$	$d^{-1}_{5/2}$	$g^{-1}_{7/2}$	$h^{-1}_{11/2}$	
$N < 82$	ϵ_{j_ν}	0.332	0.000	1.655	2.434	0.065	
	j_ν	$p_{1/2}$	$p_{3/2}$	$f_{5/2}$	$f_{7/2}$	$h_{9/2}$	$i_{13/2}$
$N > 82$	ϵ_{j_ν}	1.363	0.8537	2.0046	0.000	$\epsilon_{h_{9/2}}$	2.690
	$G_{0\nu}$	$G_{2\nu}$	κ_ν	$G_{0\pi}$	$G_{2\pi}$	κ_π	$\kappa_{\pi\nu}$
$N \leqslant 82$	0.17	0.021	0.04	0.18	0.018	0.039	+0.08
$N > 82$	0.11	0.01	0.02	0.13	0.024	0.05	−0.08

the numbers of valence neutrons. For $N = 83$ and $N = 85$, $\epsilon_{h_{9/2}} = 1.5609$ and 0.9503 MeV, which are taken from the corresponding experimental excitation energies of ^{133}Sn and ^{135}Sn. For $N = 87$, no experimental data is available for ^{137}Sn, so $\epsilon_{h_{9/2}} = 0.6956$ MeV comes from fitting the experimental energy levels of ^{139}Te.

The $E2$ transition operator is defined by $T(E2) = e_\pi Q_\pi + e_\nu Q_\nu$, where e_π and e_ν correspond to the effective charges of valence proton and valence neutron. The $B(E2)$ value in units of W.u. is given by

$$B(E2; J_i \to J_f) = \mathcal{C} \times (e_\pi \chi_\pi + e_\nu \chi_\nu)^2, \tag{2}$$

with

$$\mathcal{C} = \frac{2J_f + 1}{2J_i + 1} \times \frac{r_0^4}{5.94 \times 10^{-6} \times A^{4/3}}.$$

Here, reduced matrix element $\chi_\sigma = \langle \beta_f, J_f || Q_\sigma || \beta_i, J_i \rangle$ ($\sigma = \pi, \nu$) and $r_0^2 = 1.012A^{1/3}$ fm^2. $|\beta_i, J_i\rangle$ is the eigenfunction carrying angular momentum J_i and the symbol β_i represents all quantum numbers other than J_i. The electric quadrupole moment is related to the $E2$ transition operator by

$$Q(J_i) = \sqrt{\frac{16\pi}{5}} C^{J_i J_i}_{J_i J_i, 20} (e_\pi \chi_\pi + e_\nu \chi_\nu) r_0^2, \tag{3}$$

with $\chi_\sigma = \langle \beta_i, J_i || Q_\sigma || \beta_i, J_i \rangle$ ($\sigma = \pi, \nu$). The magnetic dipole moment is defined by

$$\mu(J_i) = \sqrt{\frac{4\pi}{3}} C^{J_i J_i}_{J_i J_i, 10} (\xi_{l\pi} + \xi_{s\pi} + \xi_{l\nu} + \xi_{s\nu}) \mu_N, \tag{4}$$

with reduced matrix element $\xi_{l\sigma} = \langle \beta_i, J_i || g_{l\sigma} L_\sigma || \beta_i, J_i \rangle$ and $\xi_{s\sigma} = \langle \beta_i, J_i || g_{s\sigma} S_\sigma || \beta_i, J_i \rangle$ ($\sigma = \pi, \nu$). Here, L_σ and S_σ are the orbital and spin angular momenta. $g_{l\sigma}$ and $g_{s\sigma}$ correspond to the orbital and spin gyromagnetic ratios. μ_N is the nuclear magneton. The two-body interaction strengths and the parameters for calculating electromagnetic properties adopted in this paper are consistent with those of the corresponding even-even core [8].

Based on the single-particle energies in Table I, the model space we choose is as follows. For proton degree of freedom, collective S_π, D_π, G_π, I_π pairs are taken to construct the proton nucleon-pair basis. For neutron degree of freedom, collective S_ν, D_ν, K_ν pairs (or S_ν, D_ν, G_ν, I_ν, and K_ν pairs) are included in the neutron-hole (or neutron-particle) pair basis. To verify the validity of our model truncation scheme, we compare the low-lying energy levels of odd-mass $^{129-137}$Te between the NPA and the shell model (using BIGSTICK code [42], denoted by SM) by taking the same phenomenological interactions in Eq. (1). Due to the limitation of computing conditions, SM calculation of ^{139}Te is not available for the time being. It is seen in Fig. 1 that both calculations give rather similar results, and they agree well with the experimental values. This indicates that the NPA with the phenomenological interactions is very well fitted to explain low-lying states in these nuclei, especially the energies and electromagnetic properties of those states of concern (see Table II below).

III. RESULTS AND DISCUSSION

In this section, we present our calculated results of low-lying states in odd-mass Te isotopes, with neutron number from 77–87. Our results include energy levels, $E2$ transition rates, electric quadrupole moments Q, and magnetic dipole moments μ, presented in Fig. 1 and Table II. One sees that our results agree well with the experimental data on the whole. This suggests that the NPA provides a suitable theoretical framework to describe the low-lying states of these nuclei. Next, we will discuss the low-lying structure of Te isotopes from three aspects: the evolution of low-lying energy levels, the weak-coupling multiplet, and the evolution of electromagnetic moments.

A. Evolution of low-lying energy levels

In this section, we focus on the evolution of the low-lying energy levels in odd-mass Te isotopes shown in Fig. 1, and analyze its microscopic nature from the perspective of the dominant configuration of wave function.

For neutron hole-type nuclei $^{129-133}$Te, the three lowest energy levels are $3/2^+_1$, $1/2^+_1$, and $11/2^-_1$, where $11/2^-_1$ is reported to be a β-decaying isomer [13,14]. Our calculations show that these three levels have single-hole characteristics and their dominant configurations are $|(d^{-1}_{3/2})_\nu\rangle$, $|(s^{-1}_{1/2})_\nu\rangle$, and $|(h^{-1}_{11/2})_\nu\rangle$, respectively. This is consistent with the conjectures of the literature [19]. Here S pairs are omitted for short (i.e., we use abbreviations $|(S^\dagger_\pi)^{N_\pi} j^\dagger_\nu (S^\dagger_\nu)^{N_\nu}\rangle \to |j_\nu\rangle$, and j_ν corresponds to the orbit of the unpaired neutron). For ^{133}Te, there is a significant energy gap (about 700 keV) between the other low-lying levels and the above three lowest levels. The lowest energy level above $11/2^-_1$ experimentally is $(7/2^+, 5/2^-)$ located at 1096 keV. According to our calculations, this energy level is suggested to be $7/2^+_1$ and its dominant configuration is $|D_\pi(d^{-1}_{3/2})_\nu\rangle$. The $5/2^+_1$ energy level very close to it is also dominated by $|D_\pi(d^{-1}_{3/2})_\nu\rangle$. As the number of neutron holes increases to three, the above energy gap decreases rapidly to be about 300 KeV at ^{131}Te. The lower energy level is the $5/2^+_1$ state at 642 keV, dominated by $|(d^{-1}_{3/2})_\nu D_\nu\rangle$. At this point, it can be inferred that the sudden drop of the $5/2^+_1$ state from

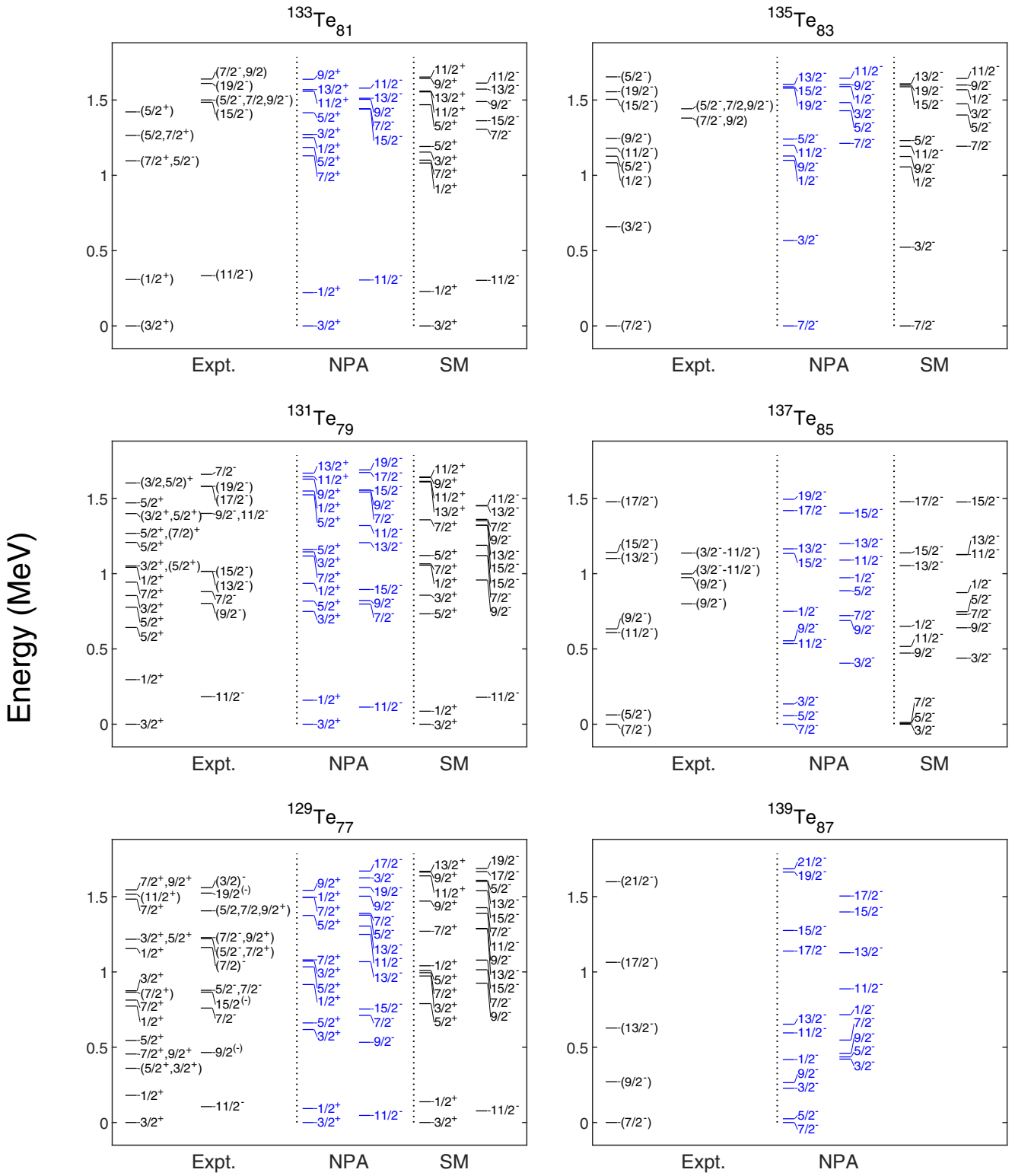

FIG. 1. Comparison of calculated and experimental excitation energies for odd-mass nuclei $^{129-133}$Te (in the left column with $N < 82$) and $^{135-139}$Te (in the right column with $N > 82$). The NPA and the shell-model calculations (denoted by SM) are performed with the same phenomenological interactions in Eq. (1). Experimental data are taken from Ref. [19,21]. Experimental levels with "( )" correspond to cases for which the spin and/or parity of the corresponding states are not well established.

TABLE II. $B(E2: J_i^\pi \to J_f^\pi)$ values (in units of W.u.), electric quadrupole moments $Q(J_i^\pi)$ (in eb), and magnetic dipole moments $\mu(J_i^\pi)$ (in μ_N) for odd-mass $^{129-139}$Te isotopes. Experimental data are from Refs. [10,19,22].

	State		$B(E2)$		$Q(J_i^\pi)$		$\mu(J_i^\pi)$	
Nuclei	J_i^π	J_f^π	Expt.	NPA	Expt.	NPA	Expt.	NPA
^{129}Te	$3/2_1^+$				0.055(13)	−0.04	0.702(4)	0.77
	$7/2_1^+$	$3/2_1^+$		14.29		+0.13		1.92
	$11/2_1^+$	$7/2_1^+$		8.45		−0.22		4.14
	$15/2_1^+$	$11/2_1^+$		6.36		−0.72		5.23
	$11/2_1^-$				+0.40(3)	+0.41	−1.091(7)	−1.18
	$15/2_1^-$	$11/2_1^-$		20.11		+0.49		−0.75
	$19/2_1^-$	$15/2_1^-$		19.94		+0.36		0.82
	$23/2_1^-$	$19/2_1^-$		5.96		−0.23		3.26
^{131}Te	$3/2_1^+$					+0.09	0.696(9)	0.84
	$7/2_1^+$	$3/2_1^+$		10.17		+0.21		2.26
	$11/2_1^+$	$7/2_1^+$		3.89		−0.26		4.24
	$15/2_1^+$	$11/2_1^+$		2.54		−0.50		5.36
	$11/2_1^-$				+0.25(14)	+0.49	−1.04(4)	−1.19
	$15/2_1^-$	$11/2_1^-$		12.70		+0.60		−0.66
	$19/2_1^-$	$15/2_1^-$		4.24		+0.14		2.31
	$23/2_1^-$	$19/2_1^-$		1.88		−0.13		3.41
	$17/2_1^-$	$13/2_1^-$	3.5(10)	2.37		+0.04		2.34
^{133}Te	$3/2_1^+$				+0.23(9)	+0.20	0.85(2)	0.89
	$7/2_1^+$	$3/2_1^+$		6.52		+0.25		2.58
	$11/2_1^+$	$7/2_1^+$		2.27		−0.32		4.41
	$15/2_1^+$	$11/2_1^+$		1.44		−0.24		5.49
	$11/2_1^-$				+0.28(14)	+0.44	(−)1.129(7)	−1.19
	$15/2_1^-$	$11/2_1^-$		4.83		+0.46		0.49
	$19/2_1^-$	$15/2_1^-$	2.56(14)	1.80		+0.08		2.72
	$23/2_1^-$	$19/2_1^-$		0.62		−0.05		3.52
^{135}Te	$7/2_1^-$				+0.29(9)	−0.29	−0.69(5)	−0.73
	$11/2_1^-$	$7/2_1^-$	>0.020	4.66		−0.13		1.02
	$15/2_1^-$	$11/2_1^-$	6.6(2)	4.63		−0.26		2.77
	$19/2_1^-$	$15/2_1^-$	3.92(20)	3.29		−0.53	−3.8(4)	3.97
^{137}Te	$7/2_1^-$					−0.18		−0.58
	$11/2_1^-$	$7/2_1^-$		10.13		−0.26		0.11
	$15/2_1^-$	$11/2_1^-$		10.72		−0.28		0.69
	$19/2_1^-$	$15/2_1^-$		4.63		−0.53		3.74
^{139}Te	$7/2_1^-$					+0.01		−0.54
	$11/2_1^-$	$7/2_1^-$		12.05		−0.19		0.27
	$15/2_1^-$	$11/2_1^-$		13.05		−0.29		1.90
	$19/2_1^-$	$15/2_1^-$		7.45		−0.57		3.77

^{133}Te to ^{131}Te is influenced by the drastic decrease of the 2_1^+ state energy between ^{134}Te and ^{132}Te, whose nature is changes from proton to neutron excitation. However, from ^{133}Te to ^{131}Te, the experimental $7/2_1^+$ energy changes little (from 1096 keV to 943 keV). This is mainly because $7/2_1^+$ state of ^{131}Te is still dominated by $|D_\pi(d_{3/2}^{-1})_\nu\rangle$ (76%) from our calculations.

The neutron-particle-type nuclei $^{135-139}$Te present faster collective development than the neutron-hole-type nuclei $^{129-133}$Te. The nucleus ^{135}Te has one valence neutron outside ^{132}Sn. In the literature [19], the configuration of its $(7/2_1^-)$ ground state is $\nu f_{7/2}$; $(3/2_1^-)$ and $(1/2_1^-)$ levels are probable $\nu p_{3/2}$ and $\nu p_{1/2}$ states, respectively. Our results are consistent with the above, and the three energy levels are dominated by

$|(f_{7/2})_\nu\rangle$, $|(p_{3/2})_\nu\rangle$, and $|(p_{1/2})_\nu\rangle$, respectively. The other low-lying states of ^{135}Te do not have single-particle characteristics with high probability in our calculations. Above the $(1/2^-_1)$ level, there are three successive levels [i.e. $(5/2^-_1)$, $(11/2^-_1)$, and $(9/2^-_1)$] that are very close in energy, all of which have a dominant configuration of $|D_\pi(f_{7/2})_\nu\rangle$. The dominant configurations $13/2^-_1$ and $15/2^-_1$ are $|G_\pi(f_{7/2})_\nu\rangle$; those of $17/2^-_1$ and $19/2^-_1$ are $|I_\pi(f_{7/2})_\nu\rangle$; that of $21/2^-_1$ is $|I_\pi(h_{9/2})_\nu\rangle$.

The nucleus ^{137}Te has two more neutrons than ^{135}Te. As can be seen from Fig. 1, the three lowest energy levels of ^{137}Te calculated are $7/2^-_1$, $5/2^-_1$, and $3/2^-_1$ in turn, which is consistent with the large-scale shell-model calculations performed using Napoli and N3LOP effective interactions [21]. Although the $3/2^-_1$ level has not been experimentally measured, the systematics of the $3/2^-_1$ excitation energies in neighboring $N = 85$ isotones supports our results. In terms of wave function, the $7/2^-_1$ ground state is still dominated by $|(f_{7/2})_\nu\rangle$; but the $5/2^-_1$ level is dominated by $|(f_{7/2})_\nu D_\nu\rangle$ (61%), and $3/2^-_1$ is by $|(f_{7/2})_\nu D_\nu\rangle$ (45%) and $|(p_{3/2})_\nu D_\nu\rangle$ (31%). Thus, as the number of neutrons increases from $N = 83$ to $N = 85$, the decrease in excitation energy of $5/2^-_1$ and $3/2^-_1$ is mainly due to the changes from proton to neutron excitation, similar to the previous discussion of the $5/2^+_1$ state from ^{133}Te to ^{131}Te. In Fig. 1, the $9/2^-_1$ and $11/2^-_1$ levels are close together. It is found that their dominant configurations are similar, i.e., $|D_\pi(f_{7/2})_\nu\rangle$ and $|(f_{7/2})_\nu D_\nu\rangle$. In contrast, the $13/2^-_1$ and $15/2^-_1$ levels are close in energies, but their structures are quite different. The $13/2^-_1$ state is dominated by the $|(h_{9/2})_\nu D_\nu\rangle$ configuration; while $15/2^-_1$ state is dominated by $|D_\pi(f_{7/2})_\nu D_\nu\rangle$, $|(f_{7/2})_\nu G_\nu\rangle$, and $|D_\pi(f_{7/2})_\nu G_\nu\rangle$. It is to be pointed out that our results largely agree with what was concluded in Refs. [20,21].

For the nucleus ^{139}Te with $N = 87$, the ground state is suggested to have spin and parity $I_\pi = 7/2^-$. The doublet $7/2^-_1$ and $5/2^-_1$ states that occur in pairs are observed in heavier $N = 87$ isotones, corresponding to an undeformed shape [11]. As can be seen in Fig. 1, our calculations reproduce these two energy levels well; their energies are very close, and dominant configurations are $|(f_{7/2})_\nu\rangle$ and $|(f_{7/2})_\nu D_\nu\rangle$, respectively. The $3/2^-_1$ level is slightly higher than $5/2^-_1$ in our calculation, since its configuration is similar to $5/2^-_1$ state. Comparing the calculated yrast levels of ^{137}Te and ^{139}Te, one specific change is the increase in the energy gap between $9/2^-_1$ and $11/2^-_1$, and between $13/2^-_1$ and $15/2^-_1$. At this point, the unpaired neutron of $9/2^-_1$ state for ^{139}Te no longer occupies mostly the $\nu f_{7/2}$ orbit, but instead occupies the $\nu h_{9/2}$ orbit, which is dominated by $|(h_{9/2})_\nu\rangle$. The unpaired neutron of the $13/2^-_1$ level still occupies mostly the $\nu h_{9/2}$ orbit like ^{137}Te, but the reduction in the single-particle energy of the $\nu h_{9/2}$ orbit results in a reduction in the $13/2^-_1$ energy. Compared with ^{137}Te, the $11/2^-_1$ and $15/2^-_1$ level positions of ^{139}Te do not change much. This is mainly due to the fact that the unpaired neutron of these two levels still mainly occupies the $\nu f_{7/2}$ orbit, and their dominant configuration changes little. In the literature [19], both $17/2^-_1$ and $21/2^-_1$ belong to the band built on $13/2^-_1$. Our results support this conclusion, and the unpaired neutron of these two levels is mainly located in the $\nu h_{9/2}$ orbit.

TABLE III. Overlaps between yrast spin-J states $|J\rangle$ of $^{129-139}$Te and weak-coupling wave functions of $|(\nu j)^{\pm1} \otimes (J_{ee}$, even-even core$)\rangle$. Here, $(\nu j)^{+1}$ or $(\nu j)^{-1}$ refers to a single valence neutron or neutron hole in the j orbit. J_{ee} is the state spin of the corresponding even-even core.

Band	$\|J\rangle$	$\|(\nu j)^{-1} \otimes (J_{ee})\rangle$	^{129}Te	^{131}Te	^{133}Te
Band A	$\|3/2^+_1\rangle$	$\|(\nu d_{3/2})^{-1} \otimes (0^+_1)\rangle$	0.97	0.97	0.97
	$\|7/2^+_1\rangle$	$\|(\nu d_{3/2})^{-1} \otimes (2^+_1)\rangle$	0.93	0.92	0.94
	$\|11/2^+_1\rangle$	$\|(\nu d_{3/2})^{-1} \otimes (4^+_1)\rangle$	0.81	*0.59*	*0.50*
	$\|15/2^+_1\rangle$	$\|(\nu d_{3/2})^{-1} \otimes (6^+_1)\rangle$	0.96	0.98	0.99
Band B	$\|11/2^-_1\rangle$	$\|(\nu h_{11/2})^{-1} \otimes (0^+_1)\rangle$	0.96	0.96	0.98
	$\|15/2^-_1\rangle$	$\|(\nu h_{11/2})^{-1} \otimes (2^+_1)\rangle$	0.96	0.96	0.95
	$\|19/2^-_1\rangle$	$\|(\nu h_{11/2})^{-1} \otimes (4^+_1)\rangle$	0.83	*0.68*	*0.52*
	$\|23/2^-_1\rangle$	$\|(\nu h_{11/2})^{-1} \otimes (6^+_1)\rangle$	0.97	0.99	1.00
	$\|J\rangle$	$\|(\nu j)^{+1} \otimes (J_{ee})\rangle$	^{135}Te	^{137}Te	^{139}Te
Band C	$\|7/2^-_1\rangle$	$\|(\nu f_{7/2})^{+1} \otimes (0^+_1)\rangle$	0.97	0.93	0.93
	$\|11/2^-_1\rangle$	$\|(\nu f_{7/2})^{+1} \otimes (2^+_1)\rangle$	0.92	0.94	0.91
	$\|15/2^-_1\rangle$	$\|(\nu f_{7/2})^{+1} \otimes (4^+_1)\rangle$	0.82	0.92	0.82
	$\|19/2^-_1\rangle$	$\|(\nu f_{7/2})^{+1} \otimes (6^+_1)\rangle$	0.99	0.97	0.94

B. Weak-coupling multiplet

In this section, we investigate the possible weak-coupling multiplet of odd-mass Te isotopes in terms of energy level, wave function, $B(E2)$ transition, electric quadrupole moments Q, and magnetic dipole moment μ. We first present the relative energies of a few yrast states in $^{129-139}$Te and the corresponding 2^+_1, 4^+_1, and 6^+_1 states in even-even Te cores in Fig. 2, where the theoretical and experimental results are on the left and right, respectively. The selected yrast states are band A $(3/2^+_1, 7/2^+_1, 11/2^+_1, 15/2^+_1)$, and band B $(11/2^-_1, 15/2^-_1, 19/2^-_1, 23/2^-_1)$ for $^{129-133}$Te; and band C $(7/2^-_1, 11/2^-_1, 15/2^-_1, 19/2^-_1)$ for $^{135-139}$Te. To understand the structures of these states, we also present in Table III the overlaps between yrast spin-J states $|J\rangle$ of $^{129-139}$Te and weak-coupling wave functions of $|(\nu j)^{\pm1} \otimes (0^+_1, 2^+_1, 4^+_1$ or 6^+_1, even-even Te core$)\rangle$. Here, $(\nu j)^{+1}$ or $(\nu j)^{-1}$ refers to a single valence neutron or neutron hole in the j orbit.

It can be seen in Figs. 2(a)–2(d) that for neutron-hole-type nuclei ($N < 82$), the relative excitation energies of each yrast states are in good agreement with the systematics of the corresponding 2^+_1, 4^+_1, and 6^+_1 states in even-even Te core, except for the $23/2^-_1$ state in Fig. 2(d). To understand the structures of these states, we analyze them within our collective nucleon-pair subspace. One sees in Table III that most overlaps are indeed very large (>0.9), indicating that these states can be well represented by the weak coupling between a collective state in the even-even core and the unpaired nucleon in a single-j orbit. For $11/2^+_1$ and $19/2^-_1$ states of ^{131,133}Te, it is interesting that their overlaps are about 0.5–0.6 for the $|(\nu j)^{-1} \otimes (4^+_1)\rangle$, and 0.7–0.8 for the $|(\nu j)^{-1} \otimes (6^+_1)\rangle$. As shown in Figs. 2(b), 2(d) the energy level spacing between 4^+_1 and 6^+_1 states is generally small (the experimental values are approximately 0.12 MeV at ^{134}Te, 0.10 MeV at ^{132}Te, and

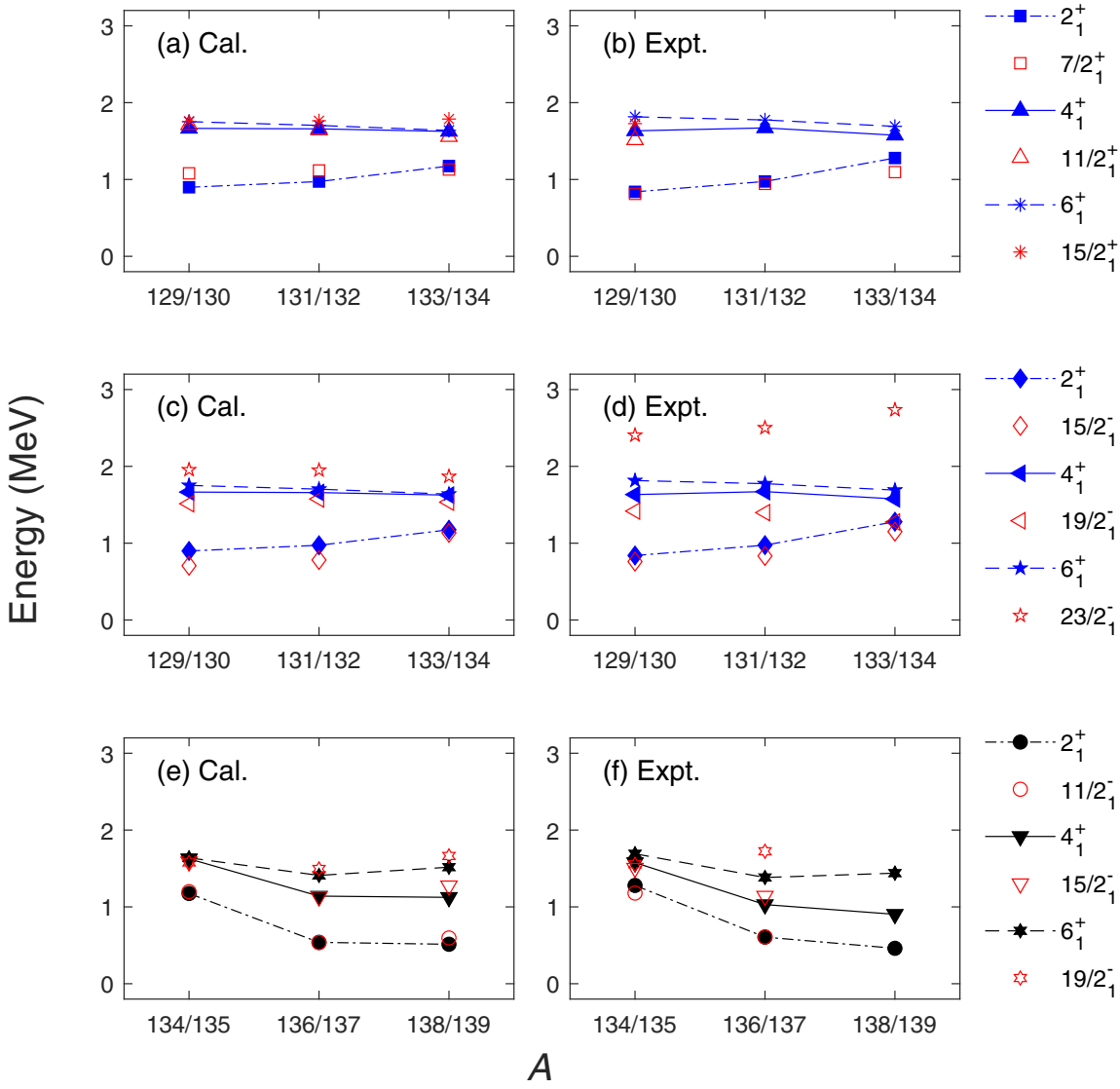

FIG. 2. The mass number (A) dependence of excitation energies (in MeV) for a few yrast states of even-even and odd-mass Te nuclei. Panels on the left are based on our calculated results, and the right on experimental results. The 2^+_1, 4^+_1, and 6^+_1 correspond to the excitation energies of even-even Te cores, represented by solid symbols. Those of odd-mass nuclei are represented by hollow symbols. (a), (b) and (c), (d) present respectively the energies of $7/2^+_1$, $11/2^+_1$, and $15/2^+_1$ states with respect to the $3/2^+_1$ and those of $15/2^-_1$, $19/2^-_1$, and $23/2^-_1$ states with respect to the $11/2^-_1$ for $^{129-133}$Te ($N < 82$). (e), (f) show the energies of $11/2^-_1$, $15/2^-_1$, and $19/2^-_1$ states relative to the $7/2^-_1$ for $^{135-139}$Te ($N > 82$). Experimental data are taken from Ref. [19].

0.18 MeV at ^{130}Te), which is mainly caused by the spin alignment of two protons in the $\pi g_{7/2}$ orbit [8]. Thus, the small overlap between the $11/2^+_1/19/2^-_1$ states and $|(\nu j)^{-1} \otimes (4^+_1)\rangle$ for ^{131,133}Te is related to the mixing effect of 4^+_1 and 6^+_1 states. The $15/2^+_1$ and $23/2^-_1$ states are little affected by the mixing effect because of the angular momentum coupling rule (i.e., $d_{3/2}$ or $h_{11/2}$ coupling with 4^+ cannot form $15/2^+$ or $23/2^-$).

In the literature [15,16], the $23/2^-_1$ level of $^{129-133}$Te is suggested to be a fully aligned $(\nu h_{11/2})^{-1} \otimes (\pi g_{7/2})^2$ state and that is exactly what we calculated. The dominant configuration of this state in the NPA is $|I_\pi(h^{-1}_{11/2})_\nu\rangle$, and the two-valence-proton configuration $(\pi g_{7/2})^2$ accounts for 99% in the collective I_π pair. Therefore, the $23/2^-_1$ state is predicted to be a good weakly coupled state $|(\nu h_{11/2})^{-1} \otimes (6^+_1)\rangle$ in Table III. However, experimental relative energies of the $23/2^-_1$ state in Fig. 2(d) are about 0.5–1 MeV higher than those of the 6^+_1 state. It should be pointed out that our calculated $23/2^-_1$ energy levels are very close to those of the shell model [16–18], both of which have large deviations from the experimental data. One sees in Fig. 2(c) that the NPA results are very close to the relative energies of the 6^+_1 state, which is more consistent with the weakly coupled picture. For the $23/2^-_1$ state, the spin and/or parity are not well established in experiment. And the shell-model calculation [18] suggested the observed first $(23/2^-)$ level at 3.070 MeV

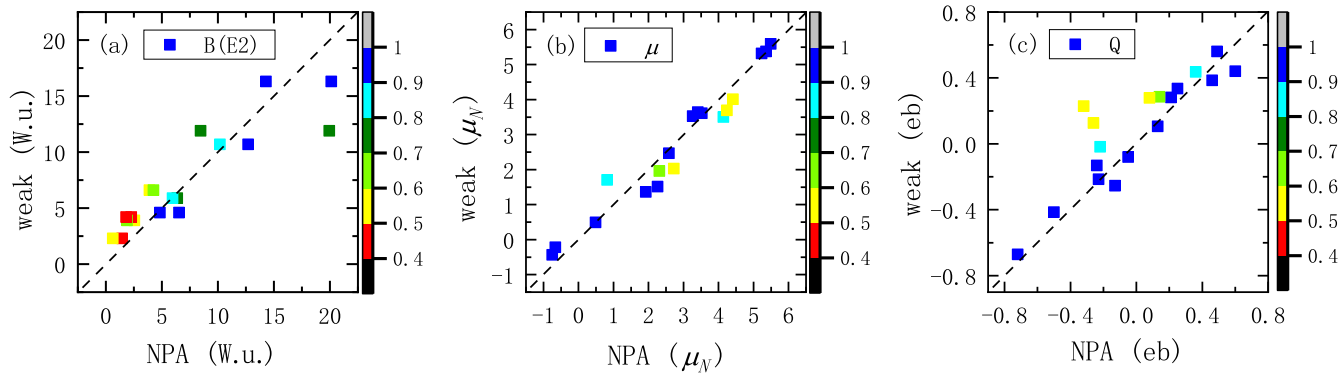

FIG. 3. Comparison of NPA predictions with weak-coupling values for the yrast states of neutron hole-type nuclei ($N < 82$) listed in Table III: (a) $B(E2)$ transitions (in W.u.), (b) magnetic dipole moment μ (in μ_N), and (c) electric quadrupole moment Q (in eb). Since $B(E2)$ transitions involves initial and final states, the color bar in panel (a) represents the product of overlap in Table III of the initial and final states of each transition. The color bars of μ and Q in panels (b), (c) represent the overlap between each state and the corresponding weak-coupling wave function.

of ^{133}Te to be the second $23/2^-$ state. Therefore, the above deviations are worthy of further study both theoretically and experimentally.

For neutron particle-type nuclei ($N > 82$) in Figs. 2(e), 2(f) the relative excitation energies of $11/2^-_1$, $15/2^-_1$, and $19/2^-_1$ states with respect to the $7/2^-_1$ level agree reasonably well with the corresponding 2^+_1, 4^+_1, and 6^+_1 states, respectively. One sees in Table III that most overlaps of band C ($7/2^-_1$, $11/2^-_1$, $15/2^-_1$, $19/2^-_1$) are above 0.9, which indicates that they can be regarded as a result of the weak coupling of the odd neutron in the $\nu f_{7/2}$ orbital to the even-even core excitations. The observed $11/2^-_1$ levels in the $N = 85$ isotones have similar characteristics [20,21].

We then discuss the weak-coupling multiplet in terms of electromagnetic properties. In the weak-coupling regime, the magnetic moment μ of state $[j \otimes J_{\rm ee}]_J$ in odd-mass nuclei can be calculated using the additivity relation [43]:

$$\mu(J) = \frac{J}{2}\left[\frac{\mu(J_{\rm ee})}{J_{\rm ee}} + \frac{\mu(j)}{j} + \left(\frac{\mu(J_{\rm ee})}{J_{\rm ee}} - \frac{\mu(j)}{j}\right) \times \frac{J_{\rm ee}(J_{\rm ee}+1) - j(j+1)}{J(J+1)}\right]. \quad (5)$$

Here, $\mu(J_{\rm ee})$ is the magnetic moment of spin-$J_{\rm ee}$ state in the corresponding even-even core. $\mu(j)$ stands for the single-particle moment with spin j. Similarly, the electric quadrupole moments $Q(J)$ in odd-mass nuclei is expressed as

$$Q(J) = \begin{pmatrix} J & 2 & J \\ -J & 0 & J \end{pmatrix}(-1)^{J_{\rm ee}+j+J}(2J+1) \times \left[\begin{Bmatrix} J_{\rm ee} & J & j \\ J & J_{\rm ee} & 2 \end{Bmatrix} \frac{Q(J_{\rm ee})}{\begin{pmatrix} J_{\rm ee} & 2 & J_{\rm ee} \\ -J_{\rm ee} & 0 & J_{\rm ee} \end{pmatrix}} + \begin{Bmatrix} j & J & J_{\rm ee} \\ J & j & 2 \end{Bmatrix} \frac{Q(j)}{\begin{pmatrix} j & 2 & j \\ -j & 0 & j \end{pmatrix}}\right], \quad (6)$$

involving the quadrupole moment of even-even core $Q(J_{\rm ee})$, the single-particle moment $Q(j)$, Wigner-3j and Wigner-6j symbols. The $B(E2)$ values governing transitions between the states $[j \otimes J_{\rm ee}]_{J_i}$ and $[j \otimes J'_{\rm ee}]_{J_f}$ can be evaluated by the same method [44]:

$$B(E2 : (jJ_{\rm ee})_{J_i} \to (jJ'_{\rm ee})_{J_f}) = \alpha \times B(E2 : J_{\rm ee} \to J'_{\rm ee}),$$

with

$$\alpha = (2J_f+1)(2J_{\rm ee}+1) \times \left[(-1)^{j+J_{\rm ee}+J_f+2}\begin{Bmatrix} j & J_{\rm ee} & J_i \\ 2 & J_f & J'_{\rm ee} \end{Bmatrix}\right]^2.$$

It can be shown that the coefficients α in the above formula are equal to 1, for the $E2$ transition rates between the states with the same single-particle spin j in Table III (that is, $7/2^+_1 \to 3/2^+_1$, $11/2^+_1 \to 7/2^+_1$, $15/2^+_1 \to 11/2^+_1$, $15/2^-_1 \to 11/2^-_1$, $19/2^-_1 \to 15/2^-_1$, and $23/2^-_1 \to 19/2^-_1$ for $N < 82$ nuclei; $11/2^-_1 \to 7/2^-_1$, $15/2^-_1 \to 11/2^-_1$, and $19/2^-_1 \to 15/2^-_1$ for $N > 82$ nuclei). This indicates that the $B(E2)$ values are approximately equal if the additional unpaired nucleon is weakly coupled to the even-even core:

$$B(E2 : (jJ_{\rm ee})_{J_i} \to (jJ'_{\rm ee})_{J_f}) = B(E2 : J_{\rm ee} \to J'_{\rm ee}). \quad (7)$$

According to the Eqs. (5)–(7), the weak-coupling $B(E2)$, μ and Q corresponding to the states listed in Table III are calculated. Here, the local single-particle moments $\mu(j)$ and $Q(j)$ are used, which are from magnetic and electric moments of the lowest states with spin j in $^{129-139}$Te. The calculated values of weak coupling are compared with those of the NPA in Table II, as shown in Figs. 3 and 4 for $N < 82$ and $N > 82$, respectively. Since $B(E2)$ transitions involves initial and final states, the color bar in Figs. 3(a), 4(a) represents the overlap product of the initial and final states of each transition. The color bars of μ and Q in Figs. 3(b), 3(c) and 4(b), 4(c) represent the corresponding overlap of each state. It can be seen that the blue data points of $B(E2)$, μ and Q basically fall on the middle diagonal, that is, their weak-coupling values are basically consistent with the NPA results. This indicates that the state with overlap greater than 0.9 can be regarded as a good weak-coupling multiplet.

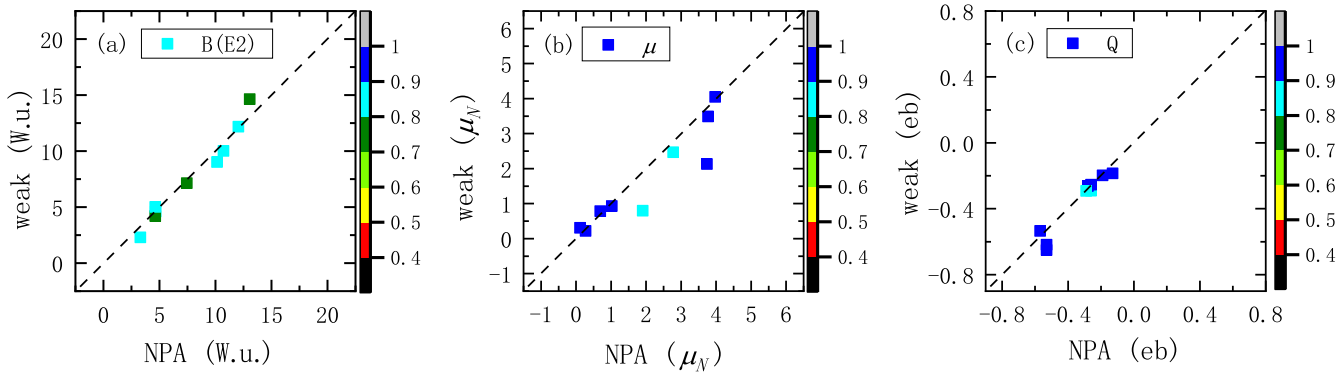

FIG. 4. Same as Fig. 3 except for the yrast states of neutron particle-type nuclei ($N > 82$) listed in Table III.

For even-even $^{128-140}$Te isotopes, the measured $B(E2; 2_1^+ \to 0_1^+)$ transitions show certain asymmetric pattern with respect to $N = 82$, which was interpreted as different core polarization below and above $N = 82$ shell [8]. According to Eq. (7), in the weak-coupling regime, the $B(E2 : (jJ_{ee})_{J_i} \to (jJ'_{ee})_{J_f})$ of odd-mass nucleus is approximately equal to the $B(E2 : J_{ee} \to J'_{ee})$ of even-even core. Therefore, it is interesting to investigate whether $B(E2)$ transitions of odd-mass nuclei have similar asymmetric pattern. In Fig. 5(a), $B(E2 : 7/2_1^+ \to 3/2_1^+)$ of $^{129-133}$Te and $B(E2 : 11/2_1^- \to 7/2_1^-)$ of $^{135-139}$Te are compared with $B(E2; 2_1^+ \to 0_1^+)$ transitions of even-even core. One sees the $E2$ ground-state transitions between odd-mass nuclei and even-even core are approximately equal, which indicates that the extra neutron in $\nu f_{7/2}$ orbit of $^{135-139}$Te (or neutron hole in $\nu d_{3/2}$ orbit of $^{129-133}$Te) has no significant effect on the reduced transition probabilities for these states. The $B(E2)$ trend of odd-mass nuclei is similar to that of even-even core. For $N < 82$, the $B(E2)$ of hole-type nuclei increases linearly with the increase of valence neutron holes. However, for $N > 82$, $B(E2)$ curve of particle-type nuclei is not linear, and the $B(E2)$ increment becomes smaller between $A = 137$ and $A = 139$. We further study the contributions of proton and neutron to $B(E2)$ values. From Eq. (2), $B(E2; J_i \to J_f) = \mathcal{C}[e_\pi \chi_\pi + e_\nu \chi_\nu]^2$ with the coefficient $\mathcal{C} \approx 0.33$ and 0.43 fm^4 for $B(E2 : 7/2_1^+ \to 3/2_1^+)$ and $B(E2 : 11/2_1^- \to 7/2_1^-)$, respectively. Therefore the proton and neutron contributions to $B(E2)$ values depend on the matrix elements $\chi_\pi^* = \sqrt{\mathcal{C}} e_\pi \chi_\pi$ and $\chi_\nu^* = \sqrt{\mathcal{C}} e_\nu \chi_\nu$. As presented in Fig. 5(b), the general trend of $B(E2)$ transitions in odd-mass nuclei are mainly determined by the neutron matrix element χ_ν^*, which is consistent with the conclusion of even-even nuclei [8].

C. Evolution of electromagnetic moments

We finally discuss the electromagnetic moments of low-lying states presented in Table II. As can be seen from this table, the observed electromagnetic moments are mainly concentrated on the ground states $3/2_1^+$ and $7/2_1^-$, as well

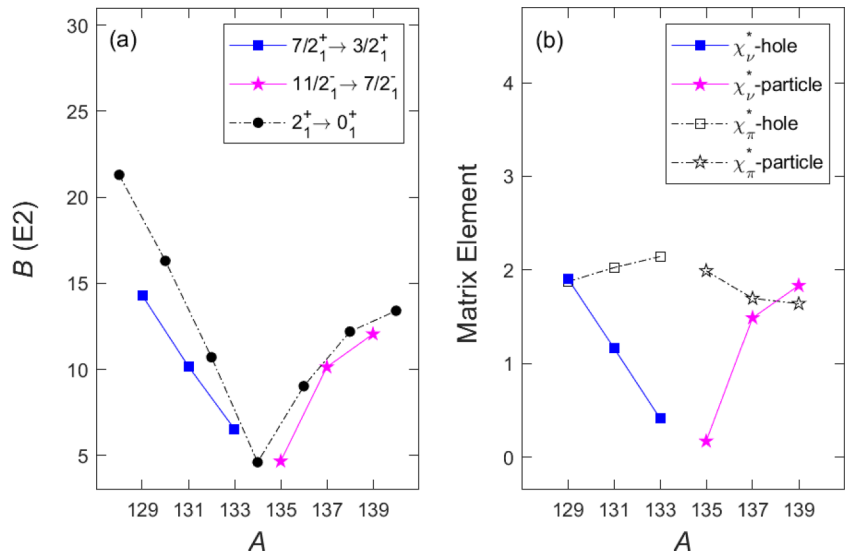

FIG. 5. (a) Comparison of $B(E2)$ transitions (in W.u.) between odd-mass Te isotopes and their even-even core, and (b) the matrix elements of proton χ_π^* and neutron χ_ν^* in odd-mass nuclei. Here, $B(E2 : 7/2_1^+ \to 3/2_1^+)$ values of $^{129-133}$Te, $B(E2 : 11/2_1^- \to 7/2_1^-)$ of $^{135-139}$Te and $B(E2 : 2_1^+ \to 0_1^+)$ of even-even $^{128-140}$Te are represented by squares, five-pointed stars, and circles, respectively.

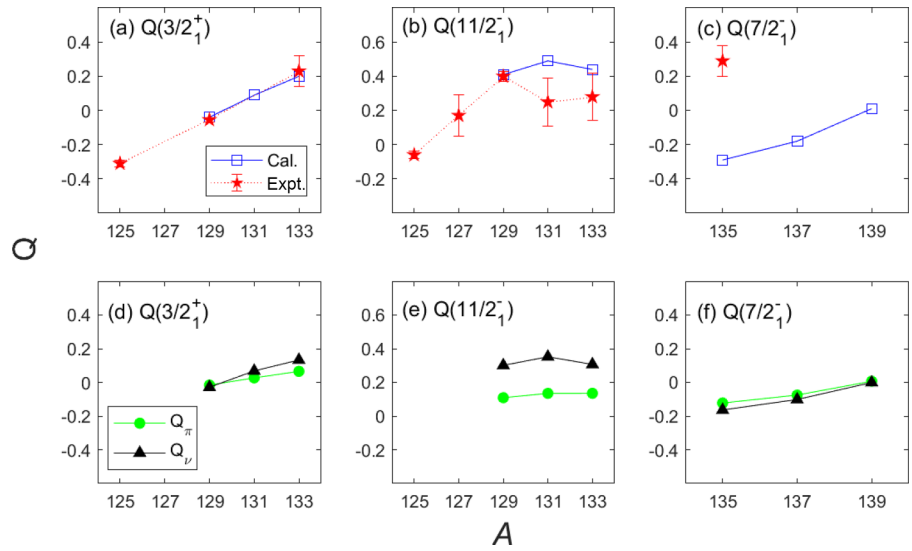

FIG. 6. The electric quadrupole moments Q (in eb) of the $3/2_1^+$, $11/2_1^-$ and $7/2_1^-$ states in the odd-mass Te isotopes. (a), (b), and (c) refer to the comparison of the experimental and calculated Q values. The experimental data are taken from Ref. [19]. (d), (e), and (f) present the proton/neutron part contributions (Q_π and Q_ν) in the Q values.

as the single neutron state $11/2_1^-$. In general, our calculations agree well with the experimental results within the error bars. In the electric multipole expansion, the electric quadrupole moment Q is an important physical quantity, which reflects the shape of the nucleus and describes the interaction between the nucleus and the external electric field. As shown in Figs. 6(a)–6(c), $Q(3/2_1^+)$, $Q(11/2_1^-)$, and $Q(7/2_1^-)$ values increase with the mass number A from negative to positive, indicating that the shape changes from oblate to prolate. It should be noted that there is one Q measurement with undetermined sign, that is $Q(3/2_1^+)$ of ^{129}Te. For this state, derived quantity is $Q_{\rm exp} = 0.055(13)e$b in experiment [45], indicating a nearly spherical structure. The magnitude of our result ($Q_{\rm cal} = -0.04$) is close to the experiment. Considering that $Q(3/2_1^+)$ value increases with A, and our result of ^{131}Te ($Q_{\rm cal} = +0.09$) is in good agreement with the quasiparticle calculation (+0.078) [45], it is reasonable for our Q value of ^{129}Te to be negative. For the $7/2_1^-$ state of ^{135}Te, the sign of the experimental and theoretical values is reversed. A similar situation also appears in shell-model calculations [24]. Their results ($Q_{\rm cal} = -0.30$ and -0.33 by using microscopic and empirical effective operators, respectively) are close to ours ($Q_{\rm cal} = -0.29$). Therefore, it is necessary to remeasure the electric quadrupole moment to clarify the true structure of this state. We further analyze the contributions of the proton and neutron components. From Eq. (3), Q can be divided into a proton part and a neutron part, i.e., $Q = Q_\pi + Q_\nu$. As presented in Figs. 6(d)–6(f), for the two ground states $3/2_1^+$ and $7/2_1^-$, the contributions of neutron and proton are approximately equal. However, for the low-lying state $11/2_1^-$, the tendency of Q to change with A is mainly determined by the neutron part.

The magnetic dipole moment μ is related to the motion state of the nucleons in the nucleus, which directly and indirectly reflects the information of nuclear structure. The overall trends of $\mu(3/2_1^+)$, $\mu(11/2_1^-)$, and $\mu(7/2_1^-)$ values with A are presented in Figs. 7(a)–7(c), respectively. It can be seen in Figs. 7(a)–7(b) that both $\mu(3/2_1^+)$ and $|\mu(11/2_1^-)|$ values of neutron-hole-type nuclei gradually decrease as the number of valence neutron holes increases (that is, the mass number A decreases). A similar conclusion can be reached for neutron-particle-type nuclei in Fig. 7(c). Namely, the $|\mu(7/2_1^-)|$ value decreases as the valence neutron number (or mass number) increases. To understand the general trend of μ values, we analyze the contributions from their proton/neutron spin and orbital angular momentum components, i.e., $\mu = \mu_{s\pi} + \mu_{sv} + \mu_{l\pi} + \mu_{lv}$. One sees in Figs. 7(d)–7(f) that the trend of μ is mainly determined by the neutron spin part μ_{sv}. According to the single-particle model, the single-neutron state properties of the odd-mass Te isotopes are determined by the last unpaired odd neutron. In the literature, the single-neutron magnetic moments in the $d_{3/2}$, $h_{11/2}$, and $f_{7/2}$ orbits are $\mu_\nu(d_{3/2}) = +0.747(4)\mu_N$ [19], $\mu_\nu(h_{11/2}) = -1.276(5)\mu_N$ [19], and $\mu_\nu(f_{7/2}) = -1.410(1)\mu_N$ [24] (taken from $\mu_{\rm exp}$ of the lowest states with spin j in ^{131}Sn and ^{133}Sn, respectively). It can be seen that these single-neutron magnetic moments are approximately equivalent to the neutron spin part μ_{sv} in Figs. 7(d)–7(f). It should be noted in Fig. 7(f) that when $N > 82$ the proton/neutron orbital parts ($\mu_{l\pi}$ and μ_{lv}) are positive and their values cannot be ignored. The negative sign of $\mu(7/2_1^-)$ is determined by the μ_{sv}, but because orbital parts cancel out some negative values, the final value of $\mu(7/2_1^-)$ is about -0.54–-0.73 in our calculation.

IV. SUMMARY

In this paper, we have calculated the low-lying level schemes, $E2$ transitional rates, electrical quadrupole moments Q, and magnetic dipole moments μ of odd-mass Te isotopes with neutron numbers from 77–87 within the nucleon-pair approximation (NPA) of the shell model, by using the phenomenological pairing plus quadrupole interactions.

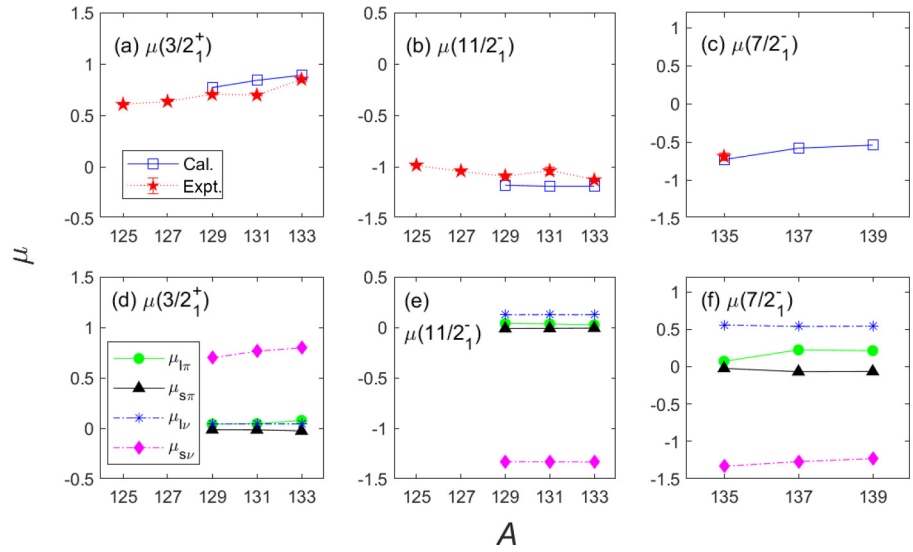

FIG. 7. Same as Fig. 6 except for the magnetic dipole moments μ (in μ_N). Here, (d), (e), and (f) present the proton/neutron spin part ($\mu_{s\pi}$, μ_{sv}) and orbital part contributions ($\mu_{l\pi}$, μ_{lv}) in the μ values.

Our results are in good agreement with available experimental data. The $B(E2)$, Q, and μ values of low-lying states are tabulated in this paper, many of which have not yet been measured for these nuclei, and they provide a quantitative reference for future experimental and theoretical studies.

The dominant configurations of yrast low-lying states are discussed in the collective nucleon-pair subspace. For neutron-hole-type nuclei $^{129-133}$Te, the $3/2_1^+$, $1/2_1^+$, and $11/2_1^-$ states have single-hole characteristics. As the mass number decreases from 133–131, the favored configuration of $5/2_1^+$ state changes from $|D_\pi(d_{3/2}^{-1})_\nu\rangle$ to $|(d_{3/2}^{-1})_\nu D_\nu\rangle$. Thus, the sudden drop of $5/2_1^+$ energy is due to the drastic decrease of the 2_1^+ energy from ^{134}Te to ^{132}Te. The $7/2_1^+$ state of both ^{133}Te and ^{131}Te are dominated by $|D_\pi(d_{3/2}^{-1})_\nu\rangle$, so there is no significant reduction in its energy value. When $N > 82$, the energy level shows a faster collective development. It is found that $7/2_1^-$, $3/2_1^-$, $1/2_1^-$ states of ^{135}Te, $7/2_1^-$, $1/2_1^-$ states of ^{137}Te, and $7/2_1^-$, $9/2_1^-$ states of ^{139}Te most likely have single-particle characteristics. We predict that both ^{137}Te and ^{139}Te have a $3/2_1^-$ state near the $5/2_1^-$ state, and the largest dominant configuration of both states is $|(f_{7/2})_\nu D_\nu\rangle$.

The weak-coupling pictures of yrast low-lying states are probed by investigating the corresponding relative excitation energy, $B(E2)$ transition, Q, and μ values. In addition, the probabilities that the states could be interpreted in terms of the weak coupling between collective even-even core and the unpaired particle are extracted from the NPA wave functions. By comparing the performance of $B(E2)$, Q, and μ values in the weak-coupling regime, it is found that the weak-coupling values of state with overlap greater than 0.9 are basically consistent with the NPA results. Therefore, the $3/2_1^+$, $7/2_1^+$, $15/2_1^+$, $11/2_1^-$, $15/2_1^-$, and $23/2_1^-$ states in $^{129-133}$Te; the $7/2_1^-$, $11/2_1^-$, and $19/2_1^-$ states in $^{135-139}$Te are suggested to be good weak-coupling multiplets. $B(E2: 7/2_1^+ \to 3/2_1^+)$ of $^{129-133}$Te and $B(E2: 11/2_1^- \to 7/2_1^-)$ of $^{135-139}$Te are compared with $B(E2; 2_1^+ \to 0_1^+)$ transitions of even-even core. $E2$ ground-state transitions of odd-mass nuclei are suggested to have similar asymmetric characteristics with respect to $N = 82$.

The electromagnetic moment Q and μ of $3/2_1^+$, $11/2_1^-$ states in $^{129-133}$Te, and $7/2_1^-$ state in $^{135-139}$Te, as well as the contributions of the proton and neutron components, are discussed. On the whole, $Q(3/2_1^+)$, $Q(11/2_1^-)$, and $Q(7/2_1^-)$ values increase with A. For the ground states $3/2_1^+$ and $7/2_1^-$, the contributions of the neutron and the proton are approximately equal; but for the $11/2_1^-$ state, the neutron component contributes more. $\mu(3/2_1^+)$ and $|\mu(11/2_1^-)|$ values of neutron-hole-type nuclei (and $|\mu(7/2_1^-)|$ values of neutron-particle-type nuclei) gradually decrease as the valence nucleon number increases. Their overall trends are suggested to be given essentially by the neutron holes/neutrons in the $\nu d_{3/2}$, $\nu h_{11/2}$, and $\nu f_{7/2}$ orbits, respectively.

ACKNOWLEDGMENTS

We thank the National Natural Science Foundation of China (Grants No. 11875188, No. 12075169, No. 12322506, and No. 12105234) for financial support.

[1] X. F. Yang, S. J. Wang, S. G. Wilkins, and R. F. Garcia Ruiz, Prog. Part. Nucl. Phys. **129**, 104005 (2023).

[2] J. J. Cowan, C. Sneden, J. E. Lawler, A. Aprahamian, M. Wiescher, K. Langanke, G. Martinez-Pinedo, and F. K. Thielemann, Rev. Mod. Phys. **93**, 015002 (2021).

[3] T. Otsuka, A. Gade, O. Sorlin, T. Suzuki, and Y. Utsuno, Rev. Mod. Phys. **92**, 015002 (2020).

[4] T. Kajino, W. Aoki, A. B. Balantekin, R. Diehl, M. A. Famiano, and G. J. Mathews, Prog. Part. Nucl. Phys. **107**, 109 (2019).

[5] H. Naïdja and F. Nowacki, J. Phys.: Conf. Ser. **966**, 012061 (2018).

[6] J. M. Allmond, A. E. Stuchbery, B. A. Brown, J. R. Beene, A. Galindo-Uribarri, C. J. Gross *et al.*, Phys. Rev. C **90**, 014322 (2014).

[7] J. Terasaki, J. Engel, W. Nazarewicz, and M. Stoitsov, Phys. Rev. C **66**, 054313 (2002).

[8] H. Jiang, Y.-J. Zhou, Y. Lei, J.-J. Shen, and M. Bao, Chin. Phys. C **45**, 094103 (2021).

[9] R. B. Cakirli and R. F. Casten, Phys. Rev. Lett. **96**, 132501 (2006).

[10] G. Simpson, J. M. Regis, L. Bettermann, J. Genevey, J. Jolie, U. Köster, T. Materna, T. Malkiewicz, J-F. Muraz, J. A. Pinston, B. Roussiere, and G. Thiamova, J. Phys. G: Nucl. Part. Phys. **46**, 065108 (2019).

[11] W. Urban, W. R. Phillips, N. Schulz, B. J. P. Gall, I. Ahmad, M. Bentaleb, J. L. Durell, M. A. Jones, M. J. Leddy, E. Lubkiewicz, L. R. Morss, A. G. Smith, and B. J. Varley, Phys. Rev. C **62**, 044315 (2000).

[12] M. Si, R. Lozeva, H. Naïdja, A. Blanc, J.-M. Daugas, F. Didierjean, G. Duchêne, U. Köster, T. Kurtukian-Nieto, F. Le Blanc, P. Mutti, M. Ramdhane, and W. Urban, Phys. Rev. C **106**, 014302 (2022).

[13] C. T. Zhang, P. Bhattacharyya, P. J. Daly, Z. W. Grabowski, R. H. Mayer, M. Sferrazza, R. Broda, B. Fornal, W. Królas, T. Pawlat, D. Bazzacco, S. Lunardi, C. Rossi Alvarez, and G. de Angelis, Nucl. Phys. A **628**, 386 (1998).

[14] P. Bhattacharyya, P. J. Daly, C. T. Zhang, Z. W. Grabowski, S. K. Saha, B. Fornal, R. Broda, W. Urban, I. Ahmad, D. Seweryniak, I. Wiedenhöver, M. P. Carpenter, R. V. F. Janssens, T. L. Khoo, T. Lauritsen, C. J. Lister, P. Reiter, and J. Blomqvist, Phys. Rev. C **64**, 054312 (2001).

[15] J. K. Hwang, A. V. Ramayya, J. H. Hamilton, C. J. Beyer, J. O. Rasmussen, Y. X. Luo, S. C. Wu, T. N. Ginter, C. M. Folden, P. Fallon, P. M. Zielinski, K. E. Gregorich, A. O. Macchiavelli, M. Stoyer, S. J. Asztalos, A. Covello, and A. Gargano, Phys. Rev. C **65**, 034319 (2002).

[16] A. Astier, M.-G. Porquet, Ts. Venkova, Ch. Theisen, G. Duchêne, F. Azaiez, G. Barreau, D. Curien, I. Deloncle, O. Dorvaux, B. J. P. Gall, M. Houry, R. Lucas, N. Redon, M. Rousseau, and O. Stézowski, Eur. Phys. J. A **50**, 2 (2014).

[17] S. Das and M. Saha Sarkar, Nucl. Phys. A **1014**, 122262 (2021).

[18] H. K. Wang, S. K. Ghorui, Z. Q. Chen, and Z. H. Li, Phys. Rev. C **102**, 054316 (2020).

[19] http://www.nndc.bnl.gov/ensdf/.

[20] W. Urban, A. Korgul, T. Rząca-Urban, N. Schulz, M. Bentaleb, E. Lubkiewicz, J. L. Durell, M. J. Leddy, M. A. Jones, W. R. Phillips, A. G. Smith, B. J. Varley, I. Ahmad, and L. R. Morss, Phys. Rev. C **61**, 041301(R) (2000).

[21] B. Moon, A. Jungclaus, H. Naïdja, A. Gargano, R. Lozeva, C.-B. Moon *et al.*, Phys. Rev. C **103**, 034320 (2021).

[22] R. Sifi, F. Le Blanc, N. Barré, L. Cabaret, J. Crawford, M. Ducourtieux, S. Essabaa, J. Genevey, G. Huber, M. Kowalska, C. Lau, J. K. P. Lee, G. Le Scornet, J. Oms, J. Pinard, B. Roussiére, J. Sauvage, M. Seliverstov, and H. Stroke, Hyperfine Interact. **171**, 173 (2006).

[23] G. White, J. Rikovska, N. J. Stone, J. Copnell, I. S. Towner, A. M. Oros, K. Heyde, B. Fogelberg, L. Jacobsson, and F. Gustavsson, Nucl. Phys. A **640**, 322 (1998).

[24] L. V. Rodríguez, D. L. Balabanski, M. L. Bissell, K. Blaum, B. Cheal, G. DeGregorio *et al.*, Phys. Rev. C **102**, 051301(R) (2020).

[25] B. Fornal, R. Broda, P. J. Daly, P. Bhattacharyya, C. T. Zhang, Z. W. Grabowski, I. Ahmad, D. Seweryniak, I. Wiedenhöver, M. P. Carpenter, R. V. F. Janssens, T. L. Khoo, T. Lauritsen, C. J. Lister, P. Reiter, and J. Blomqvist, Phys. Rev. C **63**, 024322 (2001).

[26] J. Q. Chen, Nucl. Phys. A **626**, 686 (1997); J. Q. Chen and Y. A. Luo, *ibid.* **639**, 615 (1998); Y. M. Zhao, N. Yoshinaga, S. Yamaji, J. Q. Chen, and A. Arima, Phys. Rev. C **62**, 014304 (2000).

[27] Y. M. Zhao and A. Arima, Phys. Rep. **545**, 1 (2014).

[28] Y. M. Zhao, S. Yamaji, N. Yoshinaga, and A. Arima, Phys. Rev. C **62**, 014315 (2000).

[29] H. Jiang, G. J. Fu, Y. M. Zhao, and A. Arima, Phys. Rev. C **84**, 034302 (2011); H. Jiang, X.-L. Tang, J.-J. Shen, and Y. Lei, Chin. Phys. C **43**, 124110 (2019).

[30] H. Jiang, Y. Lei, G. J. Fu, Y. M. Zhao, and A. Arima, Phys. Rev. C **86**, 054304 (2012); H. Jiang, C. Qi, Y. Lei, R. Liotta, R. Wyss, and Y. M. Zhao, *ibid.* **88**, 044332 (2013); H. Jiang, Y. Lei, C. Qi, R. Liotta, R. Wyss, and Y. M. Zhao, *ibid.* **89**, 014320 (2014); H. Jiang, B. Li, and Y. Lei, *ibid.* **93**, 054323 (2016).

[31] Y. A. Luo and J. Q. Chen, Phys. Rev. C **58**, 589 (1998); L. Y. Jia, H. Zhang, and Y. M. Zhao, *ibid.* **75**, 034307 (2007).

[32] L. Y. Jia, H. Zhang, and Y. M. Zhao, Phys. Rev. C **76**, 054305 (2007).

[33] Z. Y. Xu, Y. Lei, Y. M. Zhao, S. W. Xu, Y. X. Xie, and A. Arima, Phys. Rev. C **79**, 054315 (2009); H. Jiang, J. J. Shen, Y. M. Zhao, and A. Arima, J. Phys. G: Nucl. Part. Phys. **38**, 045103 (2011).

[34] M. Bao, H. Jiang, Y. M. Zhao, and A. Arima, Phys. Rev. C **101**, 014316 (2020).

[35] Y. A. Luo, F. Pan, C. Bahri, and J. P. Draayer, Phys. Rev. C **71**, 044304 (2005); Y. A. Luo, F. Pan, T. Wang, P. Z. Ning, and J. P. Draayer, *ibid.* **73**, 044323 (2006).

[36] Y. M. Zhao, S. Pittel, R. Bijker, A. Frank, and A. Arima, Phys. Rev. C **66**, 041301(R) (2002); Y. M. Zhao, J. L. Ping, and A. Arima, *ibid.* **76**, 054318 (2007); Y. Lei, Z. Y. Xu, Y. M. Zhao, S. Pittel, and A. Arima, *ibid.* **83**, 024302 (2011).

[37] G. J. Fu, Y. Lei, Y. M. Zhao, S. Pittel, and A. Arima, Phys. Rev. C **87**, 044310 (2013).

[38] Y. Y. Cheng, Y. M. Zhao, and A. Arima, Phys. Rev. C **97**, 024303 (2018).

[39] B. C. He, Lei Li, Y. A. Luo, Y. Zhang, F. Pan, and J. P. Draayer, Phys. Rev. C **102**, 024304 (2020); Y. Lei, Y. Lu, and Y. M. Zhao, Chin. Phys. C **45**, 054103 (2021).

[40] G. J. Fu and Calvin W. Johnson, Phys. Lett. B **809**, 135705 (2020); G. J. Fu, Calvin W. Johnson, P. Van Isacker, and Z. Ren, Phys. Rev. C **103**, L021302 (2021); G. J. Fu and Calvin W. Johnson, *ibid.* **104**, 024312 (2021).

[41] C. Ma, X. Yin, and Y. M. Zhao, Phys. Rev. C **108**, 034308 (2023).

[42] C. W. Johnson, W. E. Ormand, K. S. McElvain, and H. Z. Shan, arXiv:1801.08432.

[43] G. Neyens, Rep. Prog. Phys. **66**, 633 (2003).

[44] R. D. Lawson, *Theory of the Nuclear Shell Model* (Clarendon Press, Oxford, 1980).

[45] I. Berkes, O. El Hajjaji, M. Fahad, B. Hlimi, G. Marest, H. Sayouty, G. Langouche, M. Van Der Heyden, and M. Tong, Hyperfine Interact. **35**, 1023 (1987).